Finite Element, Discrete-Fracture Model for Multiphase Flow in Porous Media

Jong-Gyun Kim and Milind D. Deo
Dept. of Chemical and Fuels Engineering, University of Utah, Salt Lake City, UT 84112

A new discrete-fracture multiphase flow model developed allows incorporation of fractures in a spatially explicit fashion. It is an alternative to conventional dual-porosity, dual-permeability models used most often to model fractured subsurface systems. The model was applied to a water flood on a 2-D random fracture network. A standard Galerkin finite element method was used to discretize the domain; triangular elements were used for matrix and line elements for the fractures. The finite element formulation was validated by using a commercial finite difference simulator. Results from a simple discrete-fracture model agreed reasonably well with the explicit fracture representation of the same domain. At low permeability contrasts between the matrix and the fractures, the model, as expected, predicted approximately symmetric water advance. At high permeability contrasts, the fracture network played a critical role in determining water advance and oil recovery. Significant oil bypassing was observed, particularly at higher flow rates. The oil recovery was determined by a complex interplay of the absolute matrix permeability, permeability contrast and flow rates. Fracture capillary pressure also played a significant role in determining water penetration in the matrix.

Introduction

Computer simulation of multiphase flow through fractured porous media continues to be challenging. Important applications are in the areas of contaminant transport in porous media and in oil, gas, and water flow in petroleum reservoirs. It has been recognized that most subsurface systems are fractured to a certain degree. New system characterization techniques, particularly in oil and gas reservoir engineering (Forster et al., 1998), are making it possible to map out fracture networks, at least to a limited extent. Four distinct approaches have been employed for the simulation of fluid flow in fractured porous media; explicit discrete fractures, discrete-fracture networks, single continuum, and dual continua (Bear, 1993). Development of different types of models to simulate flow through fractured formations has been underway since about 1955. Historical development of the models both in the oil industry and in the hydrogeological community has been discussed in detail by Pinder et al. (1993). Kazemi and Gilman (1993) provide a more comprehensive mathematical review of the models developed for the multiphase simulation in oil, gas, and coalbed reservoirs. Pioneering efforts of Kazemi and Gilman (1993), particularly in the development of dual-porosity models, has made possible simulation of fractured systems at the reservoir scale.

The model described in this article is specifically developed to address incorporation of fractures in a spatially explicit fashion in a given domain. The model has been developed to provide an infrastructure to utilize sophisticated fracture identification and mapping methods. Finite element reservoir simulation models are not very common. The model developed here is conceptually similar to the model developed by Dalen (1979) for nonfractured reservoirs and the hydrogeologic multiphase flow models proposed by Kaluarachchi and Parker (1989). The discrete-fracture implementation is similar in principle to the formulation described by Huyakorn and Pinder (1983), who implemented the model for a single vertical fracture. Huyakorn et al. (1994) described a three-dimensional, multiphase flow model for flow in fractured media. Slough et al. (1999) referred to a discrete-fracture model when discussing the importance of rock matrix entry pressure on dense nonaqueous-phase liquid migration

Correspondence concerning this article should be addressed to M. D. Deo.

in fractured geologic materials. Details of the model and implementation were not provided. Development and application of a discrete-fracture model to practical multiphase flow problems has not been addressed previously and is the subject of this article.

Model Development

In the discrete-fracture approach, multiphase flow equations are written for the porous matrix and for the fractures separately. Consider the flow of oil and water, the two immiscible phases, either through matrix blocks or through fractures. The governing flow equations are derived by combining Darcy's law with the equation of continuity:

Oil phase equation

$$\nabla\cdot\left[T_o\nabla(P_o-\gamma_o Z)\right]=\frac{\partial}{\partial t}\left(\phi\frac{(1-S_w)}{B_o}\right)\pm\frac{q_o}{\rho_{osc}}. \quad (1)$$

Water-phase equation

$$\nabla\cdot\left[T_w(\nabla P_o-P_c'\nabla S_w-\gamma_w Z)\right]=\frac{\partial}{\partial t}\left(\phi\frac{S_w}{B_w}\right)\pm\frac{q_w}{\rho_{wsc}}. \quad (2)$$

In Eqs. 1 and 2, the difference between phase pressures is given by the capillary pressure, which in general, is a nonlinear function of fluid saturation:

$$P_c=P_o-P_w=f(S_w) \quad (3)$$

$$S_o+S_w=1. \quad (4)$$

The transmissibilities in Eqs. 1 and 2 are given by the following expressions:

$$T_o=\frac{k_{ro}k_{\text{absolute}}}{\mu_o B_o} \quad (5)$$

$$T_w=\frac{k_{rw}k_{\text{absolute}}}{\mu_w B_w}. \quad (6)$$

In these latter equations, the relative permeabilities are also highly nonlinear functions of saturations. The main governing equations (Eqs. 1 and 2) can be formulated in terms of different sets of dependent variables (Aziz and Settari, 1979). When oil pressure and water saturation are chosen as dependent variables, Eqs. 1–3 can be combined into the following matrix equation.

$$\begin{bmatrix}0 & \nabla\cdot T_o\\ -\nabla\cdot T_w P_c' & \nabla\cdot T_w\end{bmatrix}\begin{bmatrix}\nabla S_w\\ \nabla P_o\end{bmatrix}+\begin{bmatrix}\nabla\cdot T_o & 0\\ 0 & \nabla\cdot T_w\end{bmatrix}\begin{bmatrix}-\gamma_o\nabla Z\\ -\gamma_w\nabla Z\end{bmatrix}$$
$$=\begin{bmatrix}do1 & do2\\ dw1 & dw2\end{bmatrix}\begin{bmatrix}\dfrac{\partial S_w}{\partial t}\\ \dfrac{\partial P_o}{\partial t}\end{bmatrix}+\begin{bmatrix}\dfrac{q_o}{\rho_{osc}}\\ \dfrac{q_w}{\rho_{wsc}}\end{bmatrix}. \quad (7)$$

The coefficients on the righthand side of Eq. 7 (also known as the storage matrix) can be expressed in terms of the primary variables as follows:

$$do1=-\phi\frac{1}{B_o} \quad (8a)$$

$$do2=\phi(1-S_w)\frac{\partial\left(\dfrac{1}{B_o}\right)}{\partial P_o} \quad (8b)$$

$$dw1=\phi\frac{1}{B_w} \quad (8c)$$

$$dw2=\phi S_w\frac{\partial\left(\dfrac{1}{B_w}\right)}{\partial P_o}. \quad (8d)$$

In the discrete-fracture model, identical equations are written for multiphase transport through fractures and are implemented on a local coordinate system. These are integrated with the matrix equations on the global coordinate system.

Sets of initial conditions and boundary conditions complete the equation system.

Initial Conditions:

$$P_o(x,y,0)=P_o(x,y) \quad \text{at} \quad t=0 \quad (9a)$$

$$S_w(x,y,0)=S_w(x,y) \quad \text{at} \quad t=0. \quad (9b)$$

No flow conditions (Neumann boundary conditions) are imposed at the boundaries

$$\frac{\partial P_o}{\partial x}=0, \quad \frac{\partial S_w}{\partial x}=0 \quad \text{at} \quad x=0 \quad \text{and} \quad x=x_0 \quad (10a)$$

$$\frac{\partial P_o}{\partial y}=0, \quad \frac{\partial S_w}{\partial y}=0 \quad \text{at} \quad y=0 \quad \text{and} \quad y=y_0. \quad (10b)$$

Finite element formulation was used because of the complex system geometry. The finite element discretization of the matrix and fracture flow equations is expressed in terms of nodal oil pressures and water saturations. The standard Galerkin method was employed, wherein the matrix was represented by linear triangular elements and the fractures by line elements. The shape functions representing the primary dependent variables, for the triangular and line elements, are well known (Huyakorn and Pinder, 1983). The nonconstant transmissibility terms in the flow equations are usually subjected to upstream mobility weighting (Dalen, 1979; Huyakorn and Pinder, 1983; Kaluarachchi and Parker, 1989). In the upstream weighting formulation, the generalized flux between a pair of nodes, is given by

$$(q_l)_{i,j}=\tilde{T}_l\nabla\cdot(\nabla P_l-\gamma_l\nabla Z)_{i,j}, \quad (11)$$

where the upstream weighted transmissibility is

$$\tilde{T}_l = \begin{cases} T_{l,i} & \text{if} \quad P_{l,i} - \gamma_{l,i} Z_i \geq P_{l,j} - \gamma_{l,j} Z_j \\ T_{l,j} & \text{if} \quad P_{l,j} - \gamma_{l,j} Z_j \geq P_{l,i} - \gamma_{l,i} Z_i. \end{cases} \tag{12}$$

The discretized-integral forms of Eqs. 1 and 2 are obtained by applying Green's theorem and the Galerkin formulation:

$$\begin{aligned} &- \sum^{N} \int_{\Omega} \left[\left(\tilde{T}_o \nabla \Phi \cdot \nabla \Phi \right) P_o \right] \, d\Omega + \sum^{S} \int_{S} \left(\tilde{T}_o \nabla P_o \Phi \cdot n \right) \, d\Omega \\ &\quad + \sum^{N} \int_{\Omega} \left[\left(\tilde{T}_o \bar{\gamma}_o \nabla \Phi \cdot \nabla \Phi \right) Z \right] \, d\Omega - \sum^{S} \int_{S} \left(\tilde{T}_o \bar{\gamma}_o \nabla Z \Phi \cdot n \right) \, d\Omega \\ &= \sum^{N} \int_{\Omega} \left[\left(\overline{do}_1 \Phi \cdot \Phi \right) \frac{\partial S_w}{\partial t} \right] \, d\Omega + \sum^{N} \int_{\Omega} \left[\left(\overline{do}_2 \Phi \cdot \Phi \right) \frac{\partial P_o}{\partial t} \right] \, d\Omega \\ &\quad + \sum^{N} \int_{\Omega} \left(\frac{q_o}{\rho_{osc}} \Phi \right) d\Omega \qquad \text{oil phase} \end{aligned} \tag{13}$$

$$\begin{aligned} &- \sum^{N} \int_{\Omega} \left[\left(\tilde{T}_w \nabla \Phi \cdot \nabla \Phi \right) P_o \right] \, d\Omega + \sum^{S} \int_{S} \left(\tilde{T}_w \nabla P_o \Phi \cdot n \right) \, d\Omega \\ &\quad + \sum^{N} \int_{\Omega} \left[\left(\bar{T}_w \tilde{P}_c \nabla \Phi \cdot \nabla \Phi \right) S_w \right] \, d\Omega - \sum^{S} \int_{S} \left(\tilde{T}_w \bar{P}_c' \nabla S_w \Phi \cdot n \right) \, d\Omega \\ &\quad + \sum^{N} \int_{\Omega} \left[\left(\tilde{T}_w \bar{\gamma}_w \nabla \Phi \cdot \nabla \Phi \right) Z \right] \, d\Omega - \sum^{S} \int_{S} \left(\tilde{T}_w \bar{\gamma}_w \nabla Z \Phi \cdot n \right) \, d\Omega \\ &= \sum^{N} \int_{\Omega} \left[\left(\overline{dw}_1 \Phi \cdot \Phi \right) \frac{\partial S_w}{\partial t} \right] \, d\Omega + \sum^{N} \int_{\Omega} \left[\left(\overline{dw}_2 \Phi \cdot \Phi \right) \frac{\partial P_o}{\partial t} \right] \, d\Omega \\ &\quad + \sum^{N} \int_{\Omega} \frac{q_w}{\rho_{wsc}} \Phi \, d\Omega \qquad \text{water phase}. \end{aligned} \tag{14}$$

The Neumann boundary conditions in Eq. 10, $\nabla P_o \cdot n = 0$ and $\nabla S_w \cdot n = 0$, allowed cancellation of the boundary flux terms.

The integral equations are written in matrix form as follows:

$$\begin{bmatrix} 0 & Ao \\ Aw_{pc} & Aw \end{bmatrix} \times \begin{bmatrix} S_w \\ P_o \end{bmatrix} + \begin{bmatrix} Bo1 & Bo2 \\ Bw1 & Bw2 \end{bmatrix} \times \begin{bmatrix} \dfrac{\partial S_w}{\partial t} \\ \dfrac{\partial P_o}{\partial t} \end{bmatrix} = \begin{bmatrix} Q_o \\ Q_w \end{bmatrix} + \begin{bmatrix} Go \\ Gw \end{bmatrix} \tag{15}$$

$$Ao = - \sum^{N} \int_{\Omega} \left(\tilde{T}_o \nabla \Phi \cdot \nabla \Phi \right) \, d\Omega \tag{16a}$$

$$Aw = - \sum^{N} \int_{\Omega} \left(\tilde{T}_w \nabla \Phi \cdot \nabla \Phi \right) \, d\Omega \tag{16b}$$

$$Aw_{pc} = \sum^{N} \int_{\Omega} \left(\tilde{T}_w \bar{P}_c' \nabla \Phi \cdot \nabla \Phi \right) \, d\Omega \tag{16c}$$

$$Bo1 = - \sum^{N} \int_{\Omega} \left(\overline{do} 1 \Phi \cdot \Phi \right) \, d\Omega \tag{16d}$$

$$Bo2 = - \sum^{N} \int_{\Omega} \left(\overline{do} 2 \Phi \cdot \Phi \right) \, d\Omega \tag{16e}$$

$$Bw1 = - \sum^{N} \int_{\Omega} \left(\overline{dw} 1 \Phi \cdot \Phi \right) \, d\Omega \tag{16f}$$

$$Bw2 = - \sum^{N} \int_{\Omega} \left(\overline{dw} 2 \Phi \cdot \Phi \right) \, d\Omega \tag{16g}$$

$$Q_l = \sum^{N} \int_{\Omega} \left(\frac{q_l}{\rho_{lsc}} \Phi \right) \, d\Omega \tag{16h}$$

$$G_l = - \sum^{N} \int_{\Omega} \left[\left(\tilde{T}_l \bar{\gamma}_l \nabla \Phi \cdot \nabla \Phi \right) Z \right] \, d\Omega \tag{16i}$$

Numerical oscillations are possible when solving multiphase flow problems using the pressure-saturation-dependent variable set (Dalen, 1979). To overcome this difficulty and to preserve the computational simplicity of the conventional Galerkin method, a lumping procedure was used (Dalen, 1979 and Kaluarachchi and Parker, 1989).

Elemental and global matrices were constructed using standard integration procedures. In this application, two separate sets were generated, one for the matrix system and the other for the fracture network. The two global matrices were superposed and the combined problem solved.

The resulting nonlinear set of ordinary differential equations was solved using a fully implicit formulation. The set of nonlinear equations from this formulation were solved using the inexact Newton's method. The nonlinear equations were written in terms of the residuals of the two matrix equations shown in Eq. 15. The Jacobian matrix was then calculated using numerical differentiation. Using an estimate of the primary variables, P_o (oil pressure) and S_w (water saturation), the residual vectors and the Jacobian were calculated and the correction vectors were obtained using Newton-like procedures.

Solving the Newton equation only approximately saves a great deal of computational effort. The level of inexactness can be varied to solve the Newton-like equation (Eisenstat and Walker, 1996); as more information about the function is incorporated into determining the level of inexactness, the use of the inexact formation becomes more attractive (Kim and Deo, 1999). The inexact Newton's method also facilitates the use of advanced linear solvers and parallel implementation. In this work, the system of linear equations for the calculation of correction vectors were solved using the transpose free quasi-minimal residual method (TFQMR). The method was chosen based on a comparative study of parallel linear solvers applicable to reservoir simulation (Kim and Deo, 1998).

Numerical Results

Model problem

The applicability of using the preceding scheme was tested on a two-dimensional test problem, which was created using the FracMan software (Deshowitz et al., 1995) of Golder Associates, Inc. Details of the geologic data input and the methodology of fracture network generation are discussed in detail in Forster et al. (1998). The detailed initial fracture map generated using field data is shown in Figure 1. In the

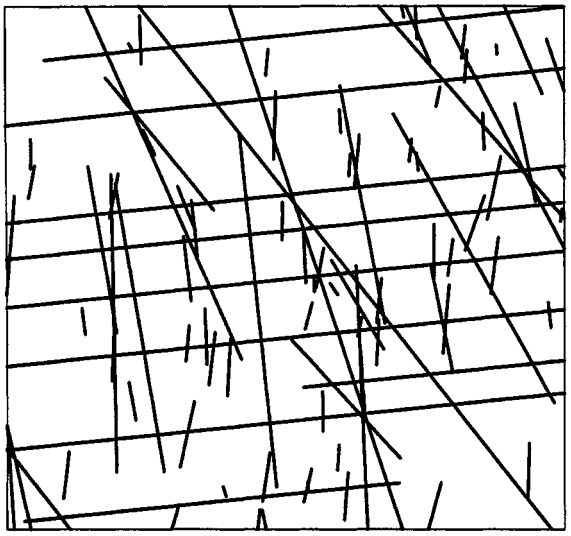

Figure 1. Original fracture map generated using field outcrop data.

Table 1. Input Data for Discrete Fracture Simulations

Porosity, fraction	0.2
Initial pressure, atm	64.6
Initial oil saturation, fraction	0.8
Stock tank oil density, g/cm^3	0.85
Stock tank water density, g/cm^3	1.0
Slope of oil formation factor vs. pres., atm^{-1}	−0.0003
Slope of oil viscosity vs. pressure, cp/atm^{-1}	0.0007
Water formation factor, RC vol./SC vol.	1.0
Water viscosity, cp	1.0

Relative permeability and capillary pressure data:

S_w	K_{rw}	K_{ro}	P_{cow} (atm)
0.0	0.00	1.0	0.61
0.1	0.00	1.0	0.61
0.2	0.00	1.0	0.61
0.3	0.0675	0.3675	0.54
0.4	0.12	0.27	0.48
0.5	0.1875	0.1875	0.41
0.6	0.27	0.12	0.34
0.7	0.3675	0.0675	0.27
0.8	1.0	0.0	0.20

creation of the discrete-fracture networks, fracture properties such as mean orientation and dispersion of orientation, mean fracture density and spacing, fracture-size statistics, and connectivity, which were collected from outcrop measurement, were used. For the test problem, about 10% of the fracture lines having dominant length were chosen from the detailed initial fracture image. The fracture network for the flow simulations is shown in Figure 2. There were a total of 193 nodes, 341 triangular elements, and 139 fracture line elements in the rectangular domain of 18.3 m by 18.3 m. Volumetric calculations were performed using a domain thickness of 0.3048 m (1 foot). Mesh generation was accomplished using the Voronoi algorithm (Fortune, 1987). The finite element grid is also shown in Figure 2. A water flood was simulated with an injection well in the northeast corner and a production well at the southwest corner, diagonally opposite. The relative permeability to oil and water were symmetrical. Relative permeabilities and other relevant properties are tabulated in Table 1. The total fluid injection and production rates were identical and kept constant over the duration of one simulation run. Several different rates and permeability contrasts were simulated. In the base-case simulation, a permeability contrast of 1:1000 between the matrix and fracture permeabilities, and an absolute matrix permeability of 1 mD was employed. The base injection rate was 0.014 m^3/day.

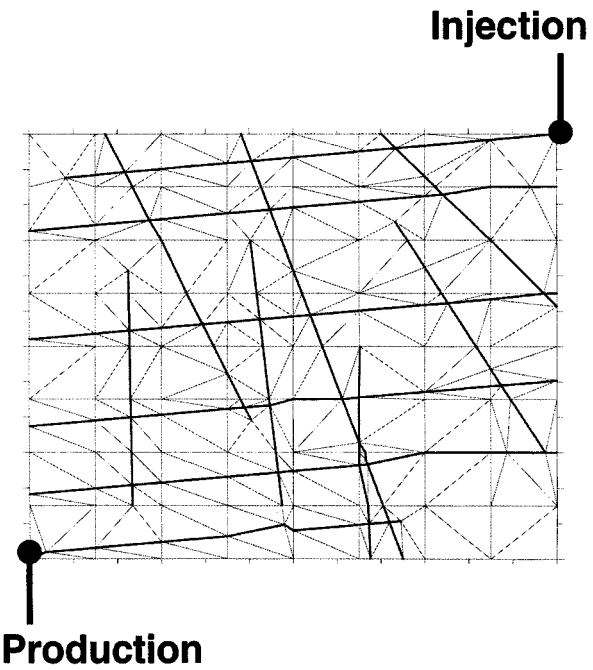

Figure 2. Discrete-fracture test domain and the finite element discretization.

The overall material balances obtained for the discrete-fracture model were excellent. The material balance error was calculated by computing the fluid volumes in place after every time step and comparing these to the fluid volumes expected by adding or subtracting fluid volumes injected or produced to volumes from the previous time step. The difference was normalized by dividing by fluid volumes in place. The cumulative material balance error after 2,000 days of injection was 0.00826% for the base-case simulation.

Validation of the model

The discrete-fracture model so developed was validated using two methods. In the first, the finite element formulation was tested on a nonfractured domain of the size described previously and results were compared to results from a finite difference model. An identical water flood problem was simulated using the two models. The finite difference simulator used was developed by the Computer Modeling Group (CMG). It was their black-oil model, IMEX (Version 1999.10). The output from a 20-by-20-grid block model was compared to the results from the straightforward finite-element discretization (regular) of the domain. Also included in this comparison are results from an irregular, unstructured grid of the same domain. This was performed to examine the ef-

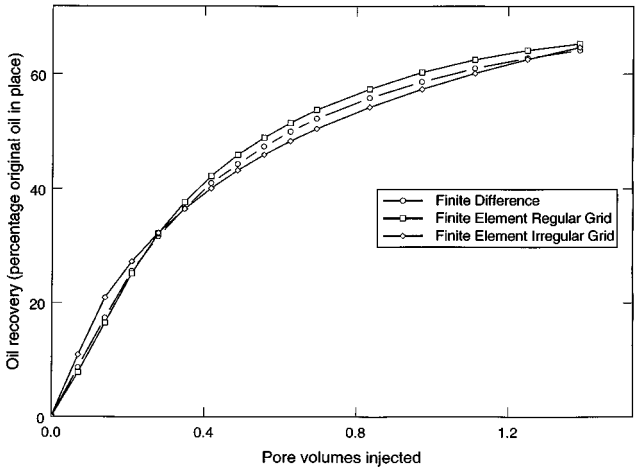

Figure 3. Recovery curves for finite element and finite difference models of the nonfractured system.

Results from a regular and an irregular finite element mesh are shown.

fect of mesh type on model results. The irregular grid was derived from the 193-node, 341-element, fractured-domain mesh with the fracture lines removed. These are single-continuum, single-porosity models. The comparison of the recovery curves from the three models is shown in Figure 3. As can be seen from the figure, there is good agreement between the results from the well-established finite difference model and the two finite element models. This shows that the finite element development, the solution method, and the numerical algorithms employed are fundamentally sound. The difference between the performance of the regular-grid finite element model and the irregular mesh model show that the finite element model results do depend on mesh type. However, this effect is not that significant for the nonfractured domain. This point is explored further in the discussion of results from the fracture model.

The Society of Petroleum Engineers (SPE) comparative solution project (Firoozabadi and Thomas, 1989) provides a comparison of the performance of ten fractured reservoir simulators. A layered system was used in the water injection example of the project. Even though all of the models were based on the dual-porosity approach, the model implementations varied significantly. As a result, the breakthrough times for the different models differed by as much as three years over a 20-year span. Thus, even though this was a comprehensive comparison study, it was inconclusive with respect to appropriateness of individual methods or specific physical mechanisms incorporated. Because of the fundamental conceptual differences between discrete-fracture models and the dual-porosity approach, it was not possible to compare the present model results with an equivalent dual-porosity model. Representation of the model domain employed using the dual-porosity approach would require assumptions that would undermine the comparison. New models are typically validated by comparing them with the fine-scale simulation of the same domain [for example, the Buckley Leverett Modified model developed by Terez and Firoozabadi (1999)]. Hence, single-porosity equivalents were chosen for comparison, both for the nonfractured finite element formulation and the discrete-fracture model.

Results from a much simpler discrete-fracture model were also compared to results from a model that allowed explicit fracture representation. The two model domains with their respective finite element discretizations are shown in Figure

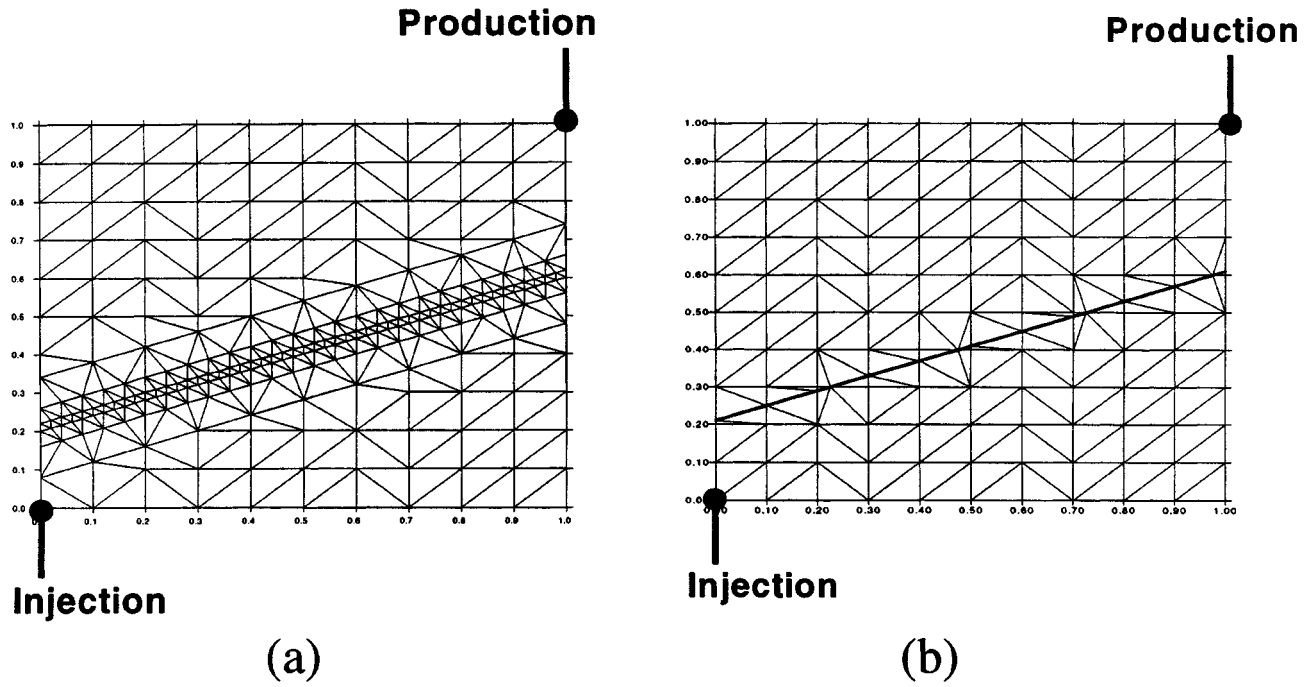

Figure 4. Simple, single-fracture problem modeled using (a) explicit fine grid representation and (b) discrete fracture approach.

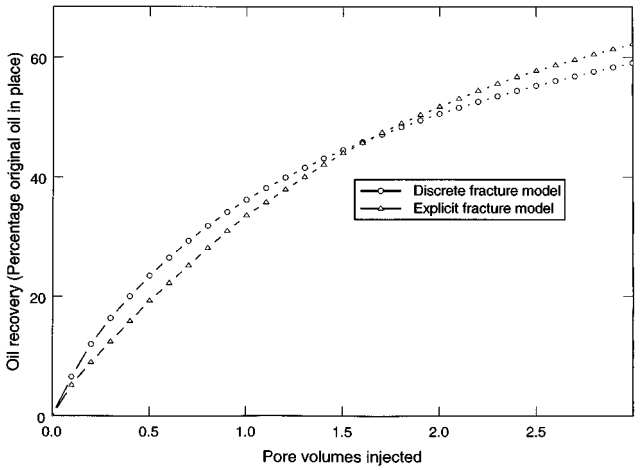

Figure 5. Oil recovery comparisons for the explicit fracture and the discrete-fracture models.

4. There were 262 nodes and 500 triangular elements in the explicit fracture representation while the discrete-fracture model divided the domain of 0.3 m by 0.3 m into 136 nodes and 228 elements, as depicted in Figure 4. The explicit fracture representation is essentially a fine-grid discretization of a domain containing a fracture. It is a single-continuum, single-porosity model that was validated earlier using a finite difference model. The model parameters used in these simulations are summarized in Table 1. A permeabilitiy contrast of 1,000 was employed. This meant that all the fine elements representing the fracture had a permeability a thousand times the permeability of the elements representing the surrounding matrix. Comparisons of the oil recovery curves for the two models are shown in Figure 5. The two curves are reasonably close. Comparison of the water saturation contours at 0.7 pore volumes (PV) injected is presented in Figure 6. The two saturation maps agree reasonably well. However, the water saturations downstream are slightly higher in the discrete-fracture model. The water velocities through the one-dimensional fracture representation in the discrete-fracture model are higher compared to the explicit fracture representation. Considering the fundamental differences between the two models, the recovery curves and the saturation maps in the two simulation methods (discrete-fracture and explicit-fracture) are still reasonably close. It should be noted that even to simulate one fracture, approximately twice the number of elements were required in the explicit-fracture representation, compared to the discrete-method. For even a small number of fractures, the explicit fracture method will become computationally impractical. Thus, a framework has been developed to simulate the presence of fractures in a spatially explicit manner using the discrete-fracture approach.

Effect of the finite-element mesh used in discrete-fracture simulations

To study the effect of the mesh used in discrete-fracture simulations, an additional simulation was performed with base-case parameters, and with a mesh that had 279 nodes, 505 elements, and 156 fracture elements. Aspect ratios (defined as the ratio of the largest to the smallest element di-

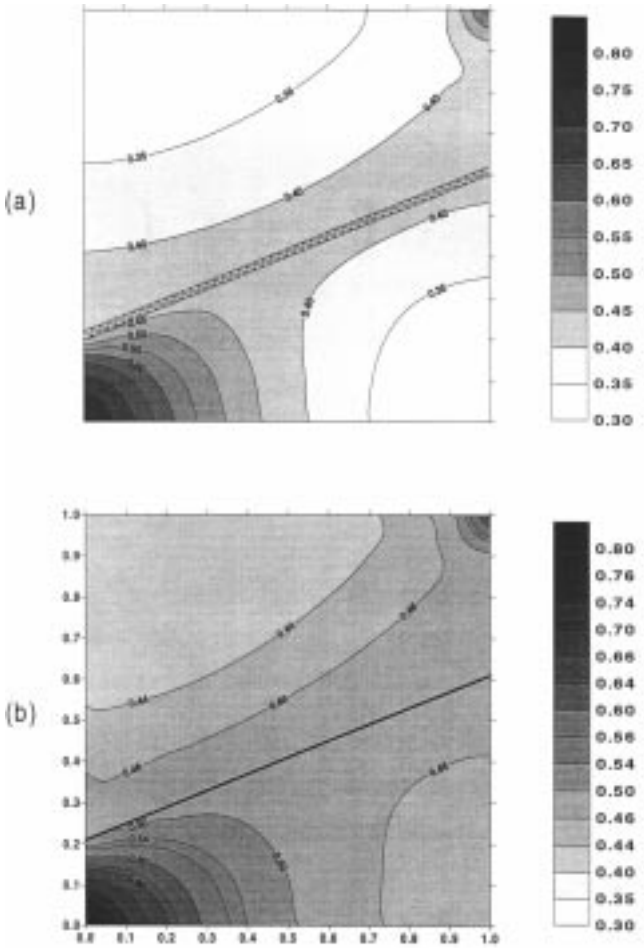

Figure 6. Water saturation contours for (a) the explicit fracture model and (b) the discrete fracture model at 0.7 PV water injected.

Absolute permeability was 1 mD and the permeability contrast was 1,000.

mension) of the elements in the newer grid were computationally more appropriate. In the new mesh, no elements had aspect ratios of larger than 6, while in the older (base-case) mesh, eight elements had aspect ratios greater than 6. The recovery curves for the two meshes are shown in Figure 7. The recovery with the larger mesh is slightly lower, possibly because the regions around fractures are better represented and the effect of the fracture network is thus more evident. Results from finite element simulations (or irregular finite difference models) do depend on mesh quality, and Figure 7 is an indication of the extent to which grid size and mesh quality affect discrete-fracture model performance.

Effect of fracture to matrix permeability contrasts

Water saturation profiles after a total of 0.7 pore volume (PV) of water injected for each of the three permeability contrasts are shown in Figure 8. Permeability contrasts (k_{fracture}:k_{matrix}) explored in this analysis represent different ratios between fracture and matrix permeability (10:1, 100:1, and 1,000:1). Other simulation parameters are given in Table 1. Since permeability contrast between the fractures and the

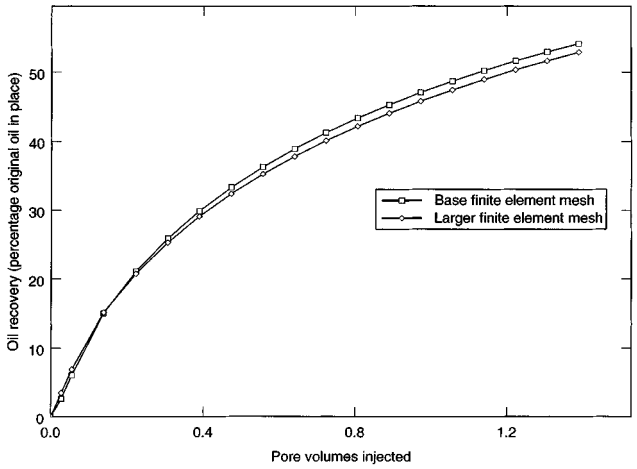

Figure 7. Oil recovery comparisons for two different finite element discretizations of the discrete-fracture domain.

matrix is small in the 10:1 case, the saturation profiles are more or less symmetrical (Figure 8). Figure 8 also shows that increasing permeability ratio to 100:1 and then to 1,000:1 causes the fractures to have a greater impact on the water flood. For a permeability contrast of 1,000:1, the flood path is uniquely fracture-network dependent. In addition, it is apparent that increasing the permeability contrasts causes a net reduction in oil recovery for a given volume of injected water (Table 2). The oil-recovery behavior is illustrated in Figure 9. As the permeability contrast increases, the water cut in the produced fluids increases more rapidly, leading to more gradual oil recovery and eventually to reduced total recovery (Table 2). Thus, localization of flow in the higher permeability fractures causes reduced sweep of oil from the intervening matrix blocks.

Mattax and Kyte (1962) studied imbibition from fractured water-drive reservoirs. When fracture permeability affected imbibition, the nature of the recovery curves at varying fracture widths was qualitatively similar to the plots shown in Figure 9. The Mattax and Kyte study is discussed in more detail while examining the effect of flow rate.

Effect of absolute matrix permeability

The absolute permeability of the matrix in all of the previous simulations was 1 mD. The effect of the absolute matrix permeability on oil recovery was examined at the highest permeability contrast (1:1,000). The recovery curve comparison is shown in Figure 10. As the absolute matrix permeability increases, the total recovery increases, as expected. Oil is also recovered at a faster rate. The water saturation contours for the two absolute permeabilities are compared in Figure 11. The fracture network plays a less significant role in determining oil recovery and fluid distributions. There is less oil bypassing and more even water saturation distribution at higher absolute matrix permeability.

Effect of injection rate

A series of simulations were performed at various injection rates and high permeability contrast to assess the effect of

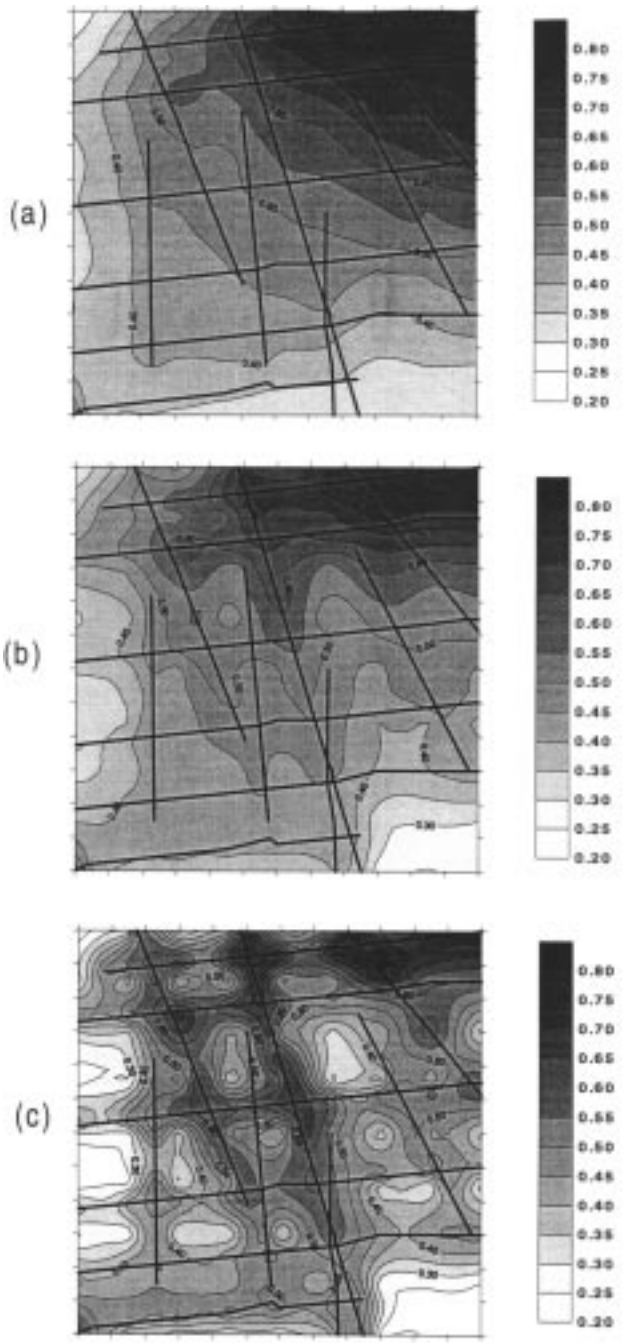

Figure 8. Effect of the matrix to fracture permeability contrast on water saturations at 0.7 PV injected.

(a) Permeability contrast—1:10, (b) permeability contrast—1:100, and (c) permeability contrast—1:1,000: absolute matrix permeability was 1 mD and injection rate 0.32 m^3/d.

flow rate on oil recovery and fluid distributions. The recovery curves for three different flow rates are compared in Figure 12. The absolute permeability in these simulations was 1 mD. The oil recoveries at 1.4 PV injected for the four flow rates are compared in Table 3. In general, as the flow rate increases, oil recovery decreases. The water saturation distribu-

Table 2. Oil Recoveries*

Model	Permeability Contrast	Rate (m^3/d)	Recovery % OOIP
Discrete fracture	10 to 1	0.014	65
Discrete fracture	100 to 1	0.014	61
Discrete fracture	1,000 to 1	0.014	54

*Percentage original oil in place, OOIP recovered after injecting 1.4 pore volumes of water at different matrix to fracture permeability ratios. Absolute permeability was 1 mD in all simulations.

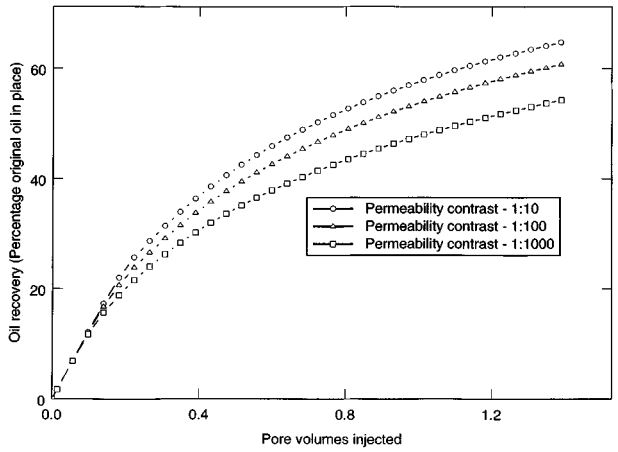

Figure 9. Oil recoveries at different matrix to fracture permeability contrast.

Absolute matrix permeability was 1 mD and flow rate 0.014 m^3/d.

tions for two of the flow rates are compared in Figure 13. It is clear from this figure that a higher injection rate leads to greater oil bypassing and thus lower recovery. Similar trends were observed for simulations performed at 100-mD absolute matrix permeability.

Mattax and Kyte (1962) identified ''a critical injection rate'' at which the water advance through the fracture is too rapid for efficient transfer of oil from the matrix to the fracture. In

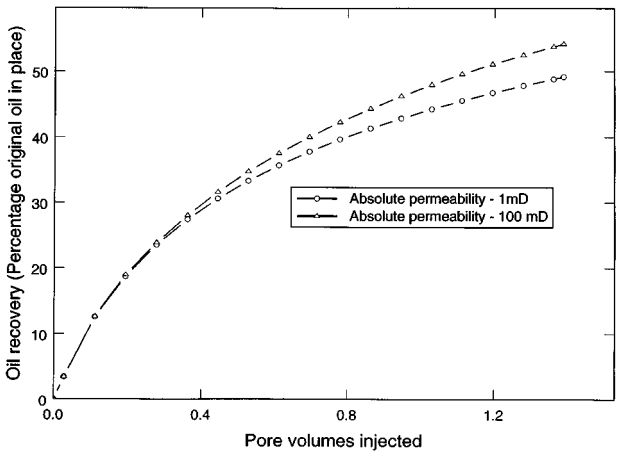

Figure 10. Oil recoveries at two different absolute matrix permeabilities.

Permeability contrast was 1:1,000 and injection rate 0.32 m^3/d.

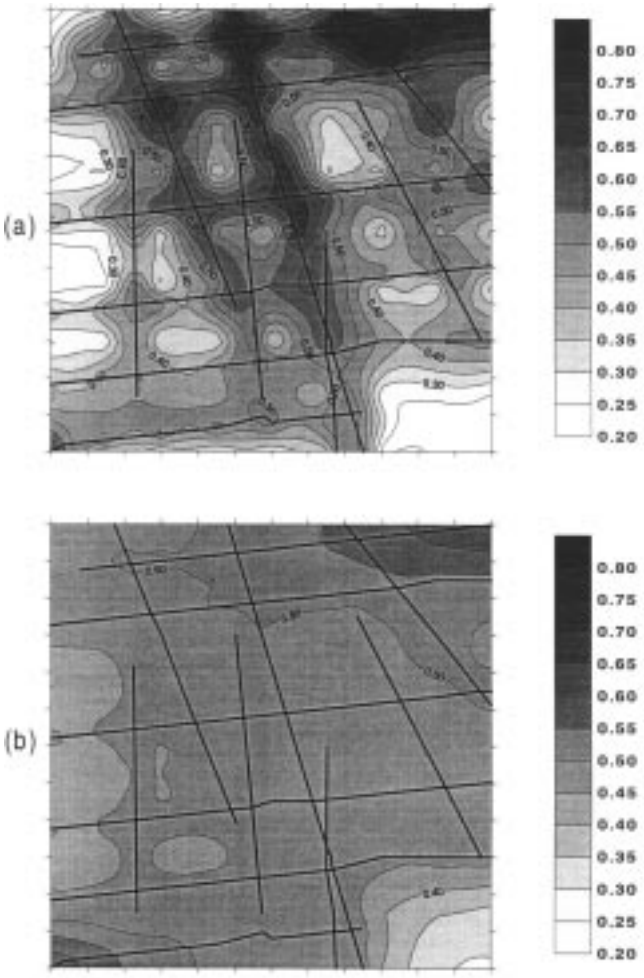

Figure 11. Water saturation contours at 0.7 PV water injected for two different absolute matrix permeabilities.

(a) 1 mD and (b) 100 mD. The matrix to fracture permeability contrast was 1:1,000 and the flow rate was 0.32 m^3/d.

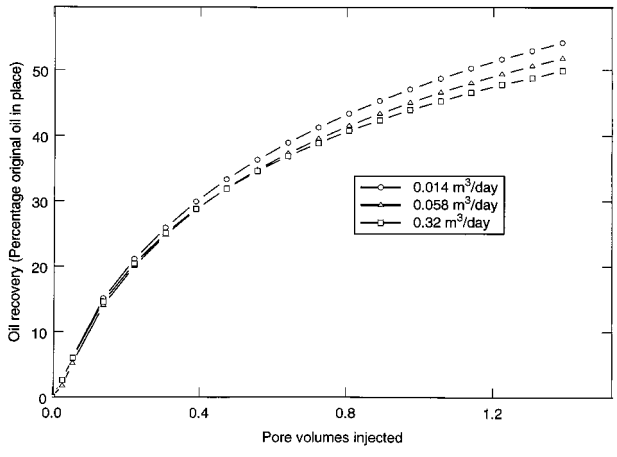

Figure 12. Effect of water injection rate on oil recoveries; absolute matrix permeability was 1 mD and the matrix to fracture permeability contrast was 1:1,000.

Table 3. Oil Recoveries*

Model	Absolute Permeability (mD)	Rate (m^3/day)	Recovery % OOIP
Discrete fracture	1	0.014	54
Discrete fracture	1	0.058	52
Discrete fracture	1	0.144	50
Discrete fracture	1	0.320	50
Discrete fracture	100	0.144	56
Discrete fracture	100	0.180	55
Discrete fracture	100	0.208	54
Discrete fracture	100	0.320	52

*Percentage original oil in place, OOIP recovered after injecting 1.4 pore volumes of water at different absolute permeabilities and injection rates: permeability contrast was 1,000 to 1 in all the simulations.

this work, even though the oil recovery was reduced with higher injection rate, it was not possible to identify a single rate at which there was a fundamental change in the oil-recovery mechanism. The Mattax and Kyte study considers only countercurrent imbibition (water imbibition and oil production from the same open fracture face). Some of the key assumptions in the study were that the fracture networks do not offer any resistance and that water advance through the fractures is uniform. Pooladi-Darvish and Firoozabadi (1997) explored the relative importance of cocurrent (water imbibition and oil production from opposing fracture faces) imbibition phenomena and observed that cocurrent imbibition is faster than countercurrent imbibition. In the discrete-fracture models, both cocurrent and countercurrent processes take place depending on the water saturations in the fracture lines surrounding each of the elements. At the same time, oil is being recovered through the matrix by viscous displacement. Results of the Mattax and Kyte (1962) experimental and analytical work apply to idealized matrix/fracture systems undergoing countercurrent imbibition. When a complex fracture network is being simulated, the recoveries are also strongly dependent on the nature of that network. The mechanistic differences between displacements at low and high rates are captured in Figure 13. At low rates, both the cocurrent and countercurrent imbibition processes are more effective and water saturations are more uniform. At higher rates, the imbibition contribution is less pronounced and there is significant bypassing.

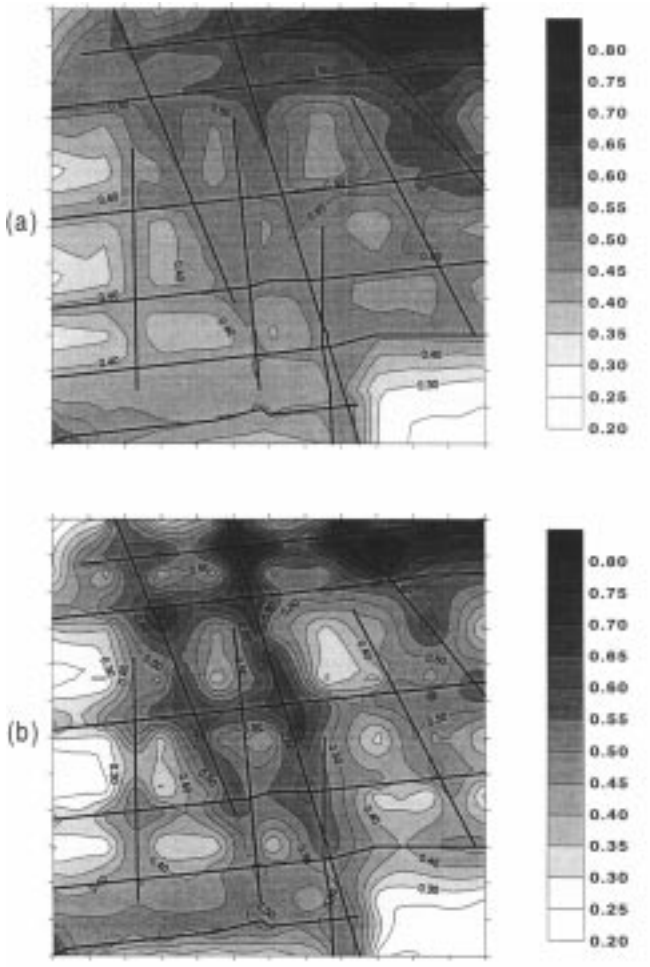

Figure 13. Water saturation contours at 0.7 PV water injected at injection rates of (a) 0.014 m^3/d and (b) 0.32 m^3/d.

The absolute matrix permeability was 1 mD and matrix to fracture permeability contrast was 1:1,000.

Effect of capillary pressure

Most of the previous studies on imbibition in fractured reservoirs assume zero capillary pressure in the fractures (Terez and Firoozabadi, 1999). The discrete-fracture model developed here allows representation of different sets of capillary pressures for the matrix and for the fractures. In addition, it also allows the input of different sets of capillary pressures in different portions of the domain. All of the previous simulations were performed with identical capillary pressure-saturation relationships in the matrix and in the fracture (Table 1). The effect of capillary pressure on oil recovery was examined by reducing the capillary pressure at the fracture nodes to 10% of the base values shown in Table 1. Capillary pressure in the fracture appeared to have a significant influence on recovery at all injection rates only at

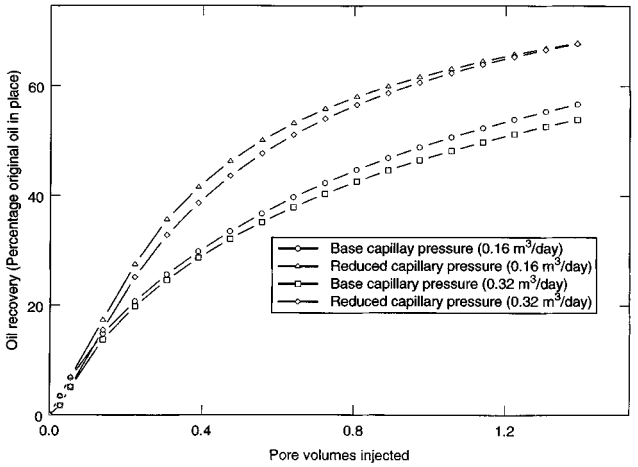

Figure 14. Effect of fracture capillary pressure on oil recoveries at two different injection rates.

Absolute permeability was 100 mD and the fracture to matrix permeability contrast ws 1:1,000.

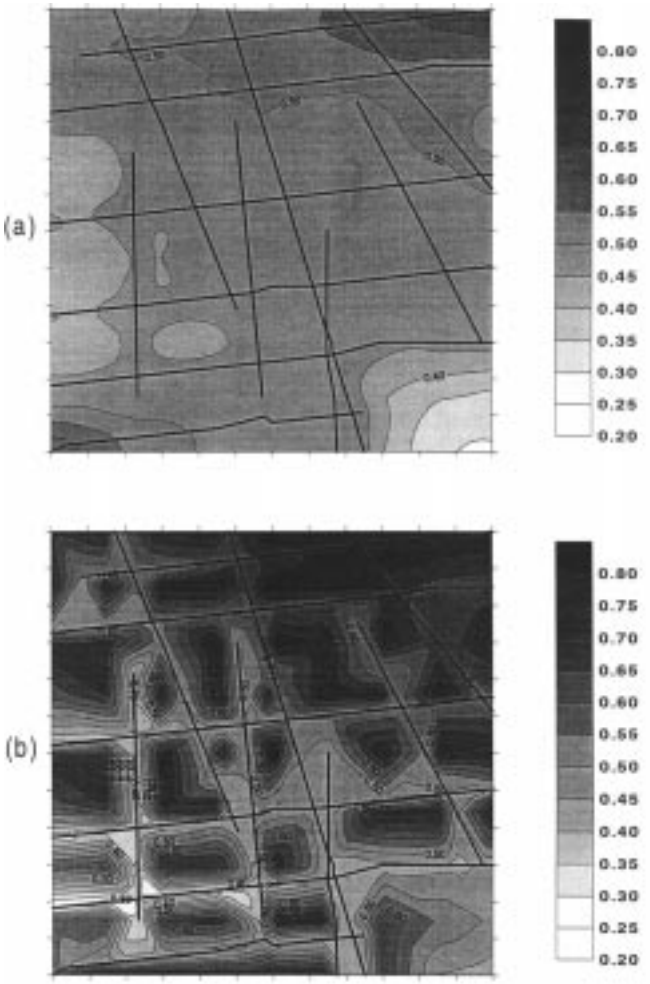

Figure 15. Water saturation contours at 0.7 PV injected for two different sets of fracture capillary pressures.

(a) Base capillary pressure (Table 1) and (b) 10% of the base capillary pressure. Absolute permeability was 100 mD, matrix to fracture permeability contrast was 1,000 and injection rate 0.32 m^3/d.

high matrix permeability. Oil recoveries at the two sets of capillary pressures are plotted in Figure 14. The matrix permeability in these simulations was 100 mD. At lower fracture capillary pressure, water appears to imbibe more efficiently into the matrix, driving oil into the fracture network. This is true for both the low and the high flow rates. The saturation maps at the two capillary pressure sets clearly illustrate this point (Figure 15). With the injection/production shut off, imbibition (mostly countercurrent) continues and there is a redistribution of water. This redistribution is more pronounced at lower capillary pressures in the fractures (higher capillary pressure contrast between matrix and fractures). When the matrix permeability is reduced to 1 mD, and at high flow rate, there is little change in oil recovery when the fracture capillary pressure is reduced. However, when the flow rate is lower, more oil is recovered at lower fracture capillary pressure (Figure 16). Since countercurrent imbibition is slower (Pooladi-Darvish and Firoozabadi, 1997), the effect of higher

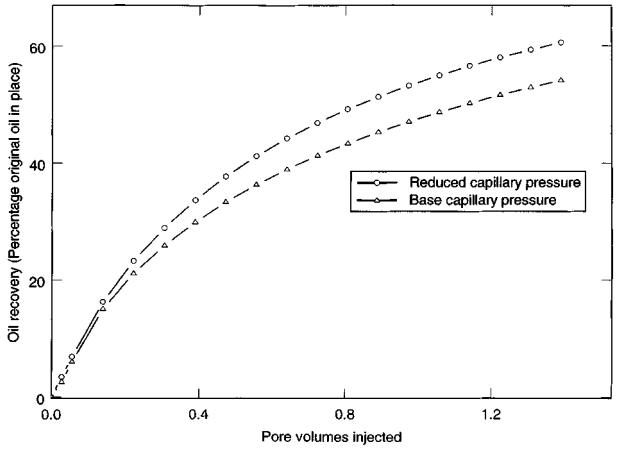

Figure 16. Oil recoveries at two sets of fracture capillary pressures: absolute permeability was 1 mD and the flow rate was 0.014 m^3/d.

The matrix to fracture permeability contrast was 1,000.

imbibition is more evident when the flow rate through the system is lower.

Conclusions

A new discrete-fracture model that incorporates fractures spatially explicitly was developed and tested on a two-dimensional data set. A diagonally oriented water flood was simulated. The nonfractured, finite element model was validated using a finite difference, commercial black-oil simulator. For a single-fracture system, the discrete-fracture model produced results comparable to the model with an explicit finite element discretization of the domain.

The discrete-fracture model was flexible, in that it was possible to use different sets of properties to represent the matrix and the fracture systems, and different portions of the domain. Several sets of simulations were performed to assess the impact of a number of input parameters. As expected, matrix-to-fracture permeability contrast played a dominant role in determining oil recovery. At high contrast (1:1,000), there was considerable oil bypassing and reduced oil recovery. At higher injection rates, the bypassing was even more pronounced. As the matrix absolute permeability increased, the fracture network played a less dominant role. Reducing the capillary pressure in the fractures generally increased oil recovery and had more significant effect when the matrix permeability was higher.

The discrete-fracture model developed in this article is an alternative to conventional dual-porosity or dual-permeability models, and can be used when detailed fracture network information is available. It allows a much finer examination of the multiphase displacement processes in fractured porous media than has been possible through models that represent fractures as uniform orthogonal networks.

Acknowledgments

The authors gratefully acknowledge financial support from the U.S. Department of Energy through a subcontract from BDM Oklahoma

(G4S51734). The authors also thank Dr. Forster of the Department of Geology and Geophysics, University of Utah, and Dr. Nielson of the Energy & Geosciences Institute, University of Utah, for their valuable input during this project. The University of Utah is a special member of the CMG (Computer Modeling Group) Consortium and would like to acknowledge the use of the IMEX black oil simulator developed by CMG Inc., Calgary, Canada.

Notation

B_l = fluid formation volume factor of phase l
k_{absolute} = absolute permeability
k_{rl} = relative permeability of phase l
P_l = pressure of phase l
q_l/ρ_{1SC} = volume produced or injected (of phase 1) per unit time per unit reservoir volume
t = time
x, y = dimensions in the Cartesian coordinate system
Z = elevation
γ_l = density of phase l in terms of pressure/distance
μ_l = viscosity of phase l
ϕ = porosity
Φ = shape function for finite element
Ω = finite element domain
∇ = difference operator in Cartesian coordinate system

Subscripts

o = related to oil phase
w = related to water phase
f = related to fracture
RC = reservoir condition
SC = stock tank or standard condition

Literature Cited

Aziz, K., and A. Settari, *Petroleum Reservoir Simulation* Elsevier, London (1979).

Bear, J., ''Modeling Flow and Contaminant Transport in Fractured Rocks,'' *Flow and Contaminant Transport in Fractured Rock*, J. Bear, C. F. Tsang, and G. de Marsily, eds., Academic Press, San Diego, p. 1 (1993).

Dalen, V., ''Simplified Finite Element Models for Reservoir Flow Problems,'' *Soc. Pet. Eng. J.*, **19**, 333 (1979).

Dershowitz, W., G. Lee, J. Geier, T. Foxford, P. LaPointe, and A. Thomas, ''FRACMAN User Document: Interactive Discrete Fracture Data Analysis, Geometric Modeling, and Exploration Simulation'' *FRACMAN Manual*, Golder Associates, Inc.. Richland, WA (1995).

Eisenstat, S. C., and H. F. Walker, ''Choosing the Forcing Terms in an Inexact Newton Method,'' *SIAM J. Sci. Comput.*, **17**, 16 (1996).

Firoozabadi, A., and L. K. Thomas, ''Sixth SPE Comparative Solution Project: A Comparison of Dual-Porosity Simulators,'' SPE 18741, Society of Petroleum Engineers, Richardson, TX (1989).

Forster, C. B., D. L. Nielson, and M. D. Deo, ''Characterization and Simulation of an Exhumed Fractured Petroleum Reservoir,'' Final Rep., Contract No. DE-A C22-94 PC91008, National Petroleum Technology Office, U.S. Dept. of Energy, Tulsa, OK (1998).

Fortune, S. J., ''A Sweepline Algorithm for Voronoi Diagrams,'' *Algorithmica*, **2** 153 (1987).

Huyakorn, P. A., S. Panday, and Y. S. Wu, ''A Three-Dimensional Multiphase Flow Model for Assessing NAPL Contamination in Porous and Fractured Media: 1. Formation,'' *J. Contam. Hydrol.*, **16**, 109 (1994).

Huyakorn, P. S., and G. F. Pinder, *Computational Methods in Subsurface Flow*, Academic Press, London, p. 172 (1983).

Kaluarachchi, J. J., and J. C. Parker, ''An Efficient Finite Element Method for Modeling Multiphase Flow,'' *Water Resour. Res.*, **25**, p. 43 (1989).

Kazemi, H., and J. R Gilman, ''Multiphase Flow in Fractured Petroleum Reservoirs,'' *Flow and Contaminant Transport in Fractured Rock*, J. Bear, C. F. Tsang, and G. de Marsily, eds., Academic Press, San Diego, p. 267 (1993).

Kim, J. G., and M. D. Deo, ''Inexact Newton-Krylov Methods for the Solution of Implicit Reservoir Simulation Problems,'' *Proc. SPE Reservoir Simulation Symp.*, Houston (1999).

Kim, J., and M. D. Deo, ''High Performance Computing in Oil Reservoir Simulation,'' AIChE Meeting, Miami Beach, FL (1998).

Mattax, C. C., and J. R. Kyte, ''Imbibition Oil Recovery from Fractured Water Drive Reservoirs,'' *SPE J.*, **2**, 177 (1962).

Pinder, G. F., P. S. Huyarkorn, and E. A. Sudicky, ''Simulation of Flow and Transport in Fractured Porous Media,'' *Flow and Contaminant Transport in Fractured Rock*, J. Bear, C. F. Tsang, and G. de Marsily, eds., Academic Press, San Diego, p. 396 (1993).

Pooladi-Darvish, M., and A. Firoozabadi, ''Cocurrent and Countercurrent Imbibition in a Water-Wet Matrix Block,'' SPE 38443 Society of Petroleum Engineers, Richardson, TX (1997).

Slough, K. J., E. A. Sudicky, and P. A. Forsyth, ''Importance of Rock Matrix Entry Pressure on DNAPL Migration in Fractured Geologic Materials,'' *Ground Water*, **37**, 2 (1999).

Terez, I. E., and A. Firoozabadi, ''Water Injection in Water-Wet Fractured Porous Media: Experiments and a New Model with Modified Buckley-Leverett Theory,'' *SPE J.*, **4**, 2 (1999).

Manuscript received June 23, 1999, and revision received Dec. 31, 1999.